Crystals Formed at 293 K by Aqueous Sulfate−Nitrate−Ammonium−Proton Aerosol Particles

Julie C. Schlenker, Adam Malinowski, Scot T. Martin,* Hui-Ming Hung, and Yinon Rudich†

Division of Engineering and Applied Sciences, Harvard University, 29 Oxford Street, Pierce Hall, Room 122, Cambridge, Massachusetts 02138

Received: May 19, 2004; In Final Form: August 11, 2004

The crystals formed at 293 K by aerosol particles composed of SO_4^{2-}, NO_3^-, NH_4^+, and H^+ are determined by aerosol flow tube infrared spectroscopy. An innovative experimental protocol is employed to restore water content to the aerosol particles and thus remove the ambiguity of their physical state after exposure to low relative humidity. The six crystals formed include $(NH_4)_2SO_4$, $(NH_4)_3H(SO_4)_2$, NH_4HSO_4, NH_4NO_3, $2NH_4NO_3{\cdot}(NH_4)_2SO_4$, and $3NH_4NO_3{\cdot}(NH_4)_2SO_4$. The dependence of which crystals form on aqueous chemical composition is reported. The infrared signatures of these crystals are determined. The infrared spectra of $2NH_4NO_3{\cdot}(NH_4)_2SO_4$, and $3NH_4NO_3{\cdot}(NH_4)_2SO_4$ and their formation in aerosol particles are reported for the first time. The formation of NH_4HSO_4 and NH_4NO_3 in initially homogeneous aerosol particles is also reported for the first time: crystallization occurs only after another crystal has already formed, indicating that heterogeneous nucleation is necessary for their formation. For some chemical compositions, in a fraction of the aerosol particles, metastable crystals that form at low relative humidity reconstruct to thermodynamically stable crystals at higher relative humidity. An externally mixed aerosol results. Contact ion pairs are apparent in the infrared spectra of aerosol particles that do not crystallize even at 1% relative humidity. Taken together, our findings suggest a more diverse array and more frequent occurrence of crystalline $SO_4^{2-}-NO_3^--NH_4^+-H^+$ aerosol particles in the troposphere than currently considered in the literature.

1. Introduction

Atmospheric aerosol particles have an important direct impact on Earth's radiation budget because they absorb and scatter incoming solar radiation directly back to space.[1] Given typical dry size distributions of 50−200 nm diameter, aqueous particles scatter solar light more efficiently than do crystalline particles and thus have a greater cooling effect.[2] Therefore, to determine the magnitude of the effect of aerosol particles on radiative forcing, it is necessary to know whether atmospheric particles are crystalline or aqueous. Aerosol particle phase and the associated radiative effect can be assessed quantitatively on the global scale by employing atmospheric chemical transport models.[3−6] Moreover, aerosol particles also affect the chemistry of the atmosphere by serving as a medium for heterogeneous reactions.[7] Chemical reactions that occur on the surface of aerosol particles, such as N_2O_5 hydrolysis or SO_2 oxidation, are orders of magnitude faster for aqueous particles than for crystalline particles.[8−10]

Atmospheric particles are commonly internal mixtures of sulfate, nitrate, ammonium, other inorganic and organic ions, nondissociated organic molecules, and insoluble inclusions, such as soot or mineral dust.[7] Sulfate, nitrate, ammonium, and proton (SNA) mass is the largest contribution by anthropogenic sources to the global accumulation mode aerosol.[1] Individual atmospheric particles can be classified as one of three types: particles of dominant SNA composition with up to 0.25 mole fraction[6,11] of other material such as organic molecules (called "SNA-dominant aerosol particles" in this paper), particles of significant SNA composition and significant quantities of other chemical species, and particles containing little SNA. All three types commonly occur in the troposphere. The work reported herein is most relevant to SNA-dominant aerosol particles. We specifically report on "SNA aerosol particles" (viz. 0.0 mole fraction of other species), and our results provide a baseline against which the behavior of SNA-dominant aerosol particles can be evaluated.[6]

The chemical composition of particles with varying amounts of SO_4^{2-}, NO_3^-, NH_4^+, and H^+ can be described in $X-Y$ space.[6] Coordinate X is the fraction of cations due to ammonium, with the balance coming from proton. Coordinate Y is the fraction of anions due to sulfate, with the balance coming from nitrate. For example, $[X, Y] = [1, 1]$ corresponds to ammonium sulfate, and $[X, Y] = [1, 0.5]$ is an equimolar mixture of ammonium sulfate and ammonium nitrate. Within this system, seven different crystals are reported for bulk volumes of material at equilibrium,[12] including $(NH_4)_2SO_4$ (AS), $(NH_4)_3H(SO_4)_2$ (LET), NH_4HSO_4 (AHS), NH_4NO_3 (AN), $2NH_4NO_3{\cdot}(NH_4)_2SO_4$ (2AN·AS), $3NH_4NO_3{\cdot}(NH_4)_2SO_4$(s) (3AN·AS), and $NH_4HSO_4{\cdot}NH_4NO_3$ (AN·AHS).

Predictions of aerosol particle phase require knowledge of the deliquescence relative humidity (DRH), the crystallization relative humidity (CRH), and the ambient relative humidity (RH) history.[13] The DRH and CRH values depend on particle chemical composition. Although the DRH values of SNA aerosol particles can be predicted based on thermodynamic models,[12,14] there is currently no physical model that can successfully predict the CRH values. Instead, the CRH values must be experimentally determined, and in an earlier report we provided CRH values of SNA aerosol particles for 293 K.[15]

* To whom correspondence should be addressed. E-mail: scot_martin@harvard.edu. Web: http://www.deas.harvard.edu/~smartin.

† Department of Environmental Sciences, Weizmann Institute, Rehovot 76100, Israel.

10.1021/jp047836z CCC: $27.50
Published on Web 10/01/2004

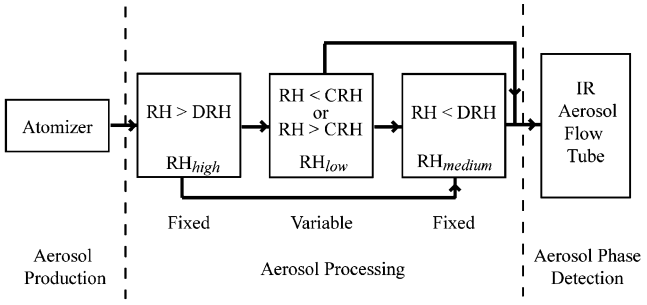

Figure 1. Schematic diagram of the experimental apparatus, including elements for aerosol generation, aerosol processing, and detection of aerosol phase. Valves are in place to program aerosol histories of (1) $RH_{high} \rightarrow RH_{low} \rightarrow RH_{medium}$, (2) $RH_{high} \rightarrow RH_{medium}$, and (3) $RH_{high} \rightarrow RH_{low}$. A comparison of the condensed-phase water content from RH history 1 versus 2 is sufficient to determine if the particles crystallize at RH_{low}.

We did not, however, identify the crystal phases formed in these particles. For any accurate effort to predict the particle phase with atmospheric chemical transport models, the crystal phases formed with decreasing RH must be known. Only when these phases are known is it possible to predict the DRH with increasing RH. In the present paper, we report the crystals formed at 293 K in SNA aerosol particles.

Previous experimental work providing information on the crystal phases formed by aerosol particles is limited to axes [*X*, 1] (i.e., mixtures of H_2SO_4 and $(NH_4)_2SO_4$) and [0, *Y*] (i.e., polar stratospheric clouds).[13] Although there is previous work on the CRH values along the [1, *Y*] axis[16,17] (i.e., mixtures of $(NH_4)_2SO_4$ and NH_4NO_3) and for mixed [*X*, *Y*] chemical compositions,[15] there are no previous reports on the crystals formed from aerosol particles of these chemical compositions. For any accurate effort to predict the SNA aerosol particle phase with atmospheric chemical transport models, the crystal phases formed with decreasing RH must be known.

2. Experimental Approach

The experimental apparatus (Figure 1) consists of three major elements, which in sequence provide for aerosol production, programming of an aerosol RH history, and detection of aerosol phase. These elements are described in detail in sections 2.1−2.3. Briefly, aerosol is produced with specific [*X*, *Y*] particle composition via atomization of an aqueous reservoir solution of the same [*X*, *Y*] chemical composition. An RH history is programmed by flowing the generated aerosol through a series of RH-controlled cells having a residence time sufficient for the water activity in the particles to equilibrate with cell RH. The processed aerosol then enters a flow cell, along the longitudinal axis of which an infrared (IR) extinction spectrum of the aerosol is recorded. The IR spectrum is diagnostic of aqueous versus crystalline particles and also indicative of which specific crystals form.

An innovation of our experimental approach, compared to previous studies employing the AFT-IR for studies of aerosol crystallization,[18−20] is the addition of a final RH-controlled cell to restore water content. Restoration of water content removes ambiguity of the physical state at low RH: within the sensitivity of IR detection, the absence of water may arise either because the aerosol liquid water content is below the minimum detection limit (i.e., metastable aqueous particles) or because the particles have crystallized. During the RH program, the aerosol is sequentially processed through environments of RH_{high} to RH_{low} to RH_{medium}. RH_{high} is above DRH(*X*,*Y*) and initializes the particles as aqueous; RH_{low} is above or below CRH(*X*,*Y*) and thus may or may not induce crystallization; RH_{medium} is below DRH(*X*,*Y*) and, if the particles have not crystallized, restores the condensed-phase water content to a level easily detected in the IR spectrum. DRH(*X*,*Y*) is calculated using a data-validated thermodynamic model.[12] Examples of specific values for ammonium sulfate are RH_{high} = 85%, RH_{low} = 30% versus 40%, and RH_{medium} = 70% (cf. Figure 2). In the usual experimental protocol for a specific [*X*, *Y*] chemical composition, RH_{high} and RH_{medium} are fixed whereas RH_{low} is variable, and the CRH value is sought by the stepwise reduction of RH_{low}.

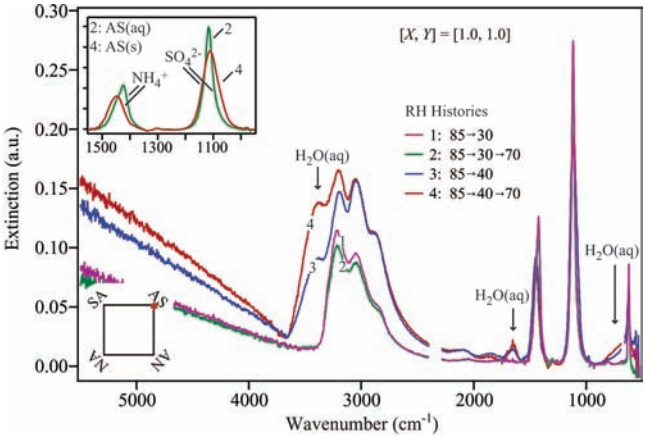

Figure 2. Infrared spectra of $(NH_4)_2SO_4$ aerosol particles (i.e., [1, 1] composition) exposed to four different RH histories at 293 K. Spectra 1 (85 → 30) and 2 (85 → 30 → 70) show no detectable condensed-phase water, indicating that the particles are crystalline. Spectra 3 (85 → 40) and 4 (85 → 40 → 70) contain condensed-phase water, indicating that the particles are aqueous. Comparison of spectra 2 and 4 illustrates the hysteresis effect. (CRH(1, 1) = 35%, DRH(1, 1) = 80%.)

Another new aspect of our experimental approach is that RH is adjusted by equilibration of the water activity of the flowing aerosol via gas-phase H_2O exchange with stationary reservoir solutions of fixed water activity. This approach has the advantage that no dilution of the aerosol with dry flow is necessary, which avoids the possibility of artifacts introduced by transient over-dried aerosol pockets when mixing dry and wet flows to obtain the desired intermediate RH. Spectral normalization, which requires the assumption of at least one invariant peak accompanying a phase transition, is not necessary. Avoiding spectral normalization is important, because our results show that peak heights change upon aerosol crystallization, in either minor or major ways depending upon the specific crystals formed.

2.1. Aerosol Production. An aerosol composed of aqueous particles is produced with a TSI 3076 atomizer (35 psi, 3 Lpm N_2, 98% RH at outlet). Reservoir solutions of specific [*X*, *Y*] composition at 1 M concentration are prepared by mixing the appropriate mole fractions of $(NH_4)_2SO_4$ and NH_4NO_3 crystals and H_2SO_4 and HNO_3 concentrated acids. Deionized (18.3 MΩ cm) and filtered (0.2 μm, hollow fiber filter) water is employed. Reservoir solutions of 1 M concentration are sufficiently concentrated that the aerosol particle mass loading is high enough for strong extinction in the IR observation cell yet sufficiently dilute so that frequent clogging of the atomizer is avoided. The mode diameter and the number concentration of the polydisperse $(NH_4)_2SO_4$ aerosol particles produced by this method are 300 nm and 6×10^6 particles/cm^3-gas, respectively, at low relative humidity.[21] We have previously shown[22] that aerosol produced via atomization has crystallization properties similar to those of aerosol produced via vapor condensation (i.e., inclusion-free particles). This result appears to rule out the

presence of significant insoluble impurities in the aqueous solutions, which are always a concern as heterogeneous nuclei.

2.2. Programming of Aerosol RH History. After generation, the aerosol flows at 3 Lpm through a set of RH-controlled cells to program an RH history (e.g., $RH_{high} \rightarrow RH_{low} \rightarrow RH_{medium}$). Bottles (4 L, Wheaton Part No. 217402) connected in series serve as RH cells. Three bottles in series constitute one cell (e.g., RH_{low}), except for RH $\leq$ 1%, for which one cell is composed of six bottles. More bottles are needed at 1% RH so that aerosol equilibration can be obtained; the residence times are 3.5 versus 7.0 min in three-bottle versus six-bottle cells, respectively. In its basin, each bottle contains 0.5 L of solution (usually sulfuric acid of 15−96% (w/w)) of fixed water activity. Holes are drilled in the bottle caps for aerosol input and output (1/2 in.) and temperature measurement (1/4 in., Pt-RTD). The aerosol input line (1/2 in. polyethylene tubing) is inserted toward the bottom of the bottle but above the solution, while the aerosol output line remains near the cap. The water activity of the aerosol particles equilibrates via gas-phase H_2O exchange with the basin solutions.

In a program of $RH_{high} \rightarrow RH_{low} \rightarrow RH_{medium}$, the second cell having RH_{low} is employed to induce crystallization. Nine different cells of RH_{low} are employed, including 1% RH and 5−40% RH in steps of 5% RH. In the usual experimental protocol, RH_{low} is increased by cell swapping, beginning at 1% RH and continuing until crystallization no longer occurs (RH_{low} > CRH). The criterion for the absence of crystallization is that the IR spectrum recorded for a program of $RH_{high} \rightarrow RH_{medium}$ is identical to that for a program of $RH_{high} \rightarrow RH_{low} \rightarrow RH_{medium}$. RH_{low} is a critical measurement in the accuracy of our results, and the maximum change of RH_{low} before and after an experiment is 2%. A secondary measurement and check on RH_{low} is performed based upon the gas-phase water absorbance in the IR spectrum.

The relative humidity inside each cell is measured using a chilled mirror hygrometer (Kahn), which has a dew point detection limit of −50 °C and an accuracy of 0.2 °C. The uncertainty in the measured RH is ±2% at 293 K. Because a constant exposure to aerosol particles would damage the hygrometer, the RH of each cell is measured with a flow of 3 Lpm N_2 before and after each experiment.

Aerosol particles having nitrate content are subject to possible HNO_3 volatilization, which could affect [*X*, *Y*] by increasing *Y*. For experiments on the same [*X*, *Y*] composition using the same number of cells, the amplitudes of the nitrate peaks do not change after exposure to low RH, thus demonstrating no detectable evaporation of HNO_3. From this result, we conclude that changes in [*X*, *Y*], if any, are minimal.

2.3. Detection of Aerosol Phase. After the programmed RH history, the aerosol flow passes into a detection cell, along the longitudinal axis of which infrared aerosol extinction spectra are recorded. The extinction spectra (software in absorbance mode, 100 scans, 2 cm^{-1} resolution) result from absorbance by gas and particles and from scattering by particles. IR spectra of gas-phase water, obtained by passage of a particle-free N_2 flow through the RH_{medium} cell, are collected before and after each aerosol experiment. These gas-phase water spectra are used to subtract the gas-phase water lines from the extinction spectra, which leave residual spectra of the condensed-phase aerosol constituents. These residual spectra are the extinction spectra reported in the present paper (i.e., Figure 2 onward).

Details of the detection cell were reported previously.[23] Briefly, the detection cell (50-mm diameter and 1-m length) is capped at both ends with AgCl windows. A collimated infrared beam passes along its axis from an infrared source (Nexus 670 FT-IR) and focuses on an active region of an MCT-A detector. One important improvement compared to our earlier description[23] is that the AgCl windows are purged with a perpendicular 1.5 Lpm N_2 flow, which reduces aerosol deposition. The purge flow is conditioned using an additional RH cell to equalize its RH with that of the entering aerosol flow. The absence of aerosol deposition onto the AgCl windows is verified after each experiment by the collection of an IR spectrum in a flow of pure N_2; this spectrum should be flat if the AgCl windows are clean.

3. Results and Discussion

3.1. Crystallization Relative Humidities. The extinction spectra shown in Figure 2 demonstrate the use of RH programming to clearly reveal phase transitions. $(NH_4)_2SO_4$ aerosol particles, which have a DRH of 80% and a CRH of 35%, are subjected to four different relative humidity histories: (1) 85 → 30%, (2) 85 → 30 → 70% (viz. $RH_{high} \rightarrow RH_{low} \rightarrow RH_{medium}$), (3) 85 → 40%, and (4) 85 → 40 → 70%. Spectrum 3 shows a significant amount of condensed-phase water at 40% RH. Spectrum 4 shows that the particles grow hygroscopically from 40 to 70% RH: there is increased absorption by condensed-phase water and these swollen particles scatter light more effectively above 4000 cm^{-1}. Comparison of spectrum 2 with spectrum 4 clearly reveals the hysteresis effect well-known for aerosol particles:[13] spectrum 2 shows no detectable condensed-phase water, even though the final RH is 70%. Spectrum 4 shows that the aqueous particles are easily detected at 70% RH. This comparison demonstrates that the particles crystallize after exposure to 30% RH, though not 40% RH, in agreement with the previous reports of a CRH value of 35%.[13]

In addition to the differences in the water content between the aqueous and the crystalline $(NH_4)_2SO_4$ particles, there are also spectral differences in the sulfate and the ammonium peak positions, heights, and multiplicities that reflect the physical state and the crystal form of the aerosol particles. The inset in Figure 2 compares the IR bands in spectra 2 (crystalline particles) and 4 (aqueous particles) in the region between 950 and 1550 cm^{-1}. The $\nu_3(SO_4^{2-})$ band at 1119 cm^{-1} sharpens upon crystallization, while the $\nu_4(NH_4^{+})$ band at 1435 cm^{-1} splits into a strong−weak overlapping doublet (1435 and 1450 cm^{-1}).[20,24]

The combination of the extinction spectra and the programming of the aerosol RH history is also useful for showing that some chemical compositions do not crystallize at 293 K, even at 1% RH. Figure 3 shows the extinction spectra collected for an NH_4HSO_4 aerosol ([0.5, 1.0], Figure 3a) and for an NH_4NO_3 aerosol ([1.0, 0.0], Figure 3b) for three different relative humidity histories: (1) $RH_{high} \rightarrow$ 1% (viz. 52 → 1%), (2) $RH_{high} \rightarrow 1\% \rightarrow RH_{medium}$ (viz. 52 → 1 → 12%), and (3) $RH_{high} \rightarrow RH_{medium}$ (viz. 52 → 12%). In history 1, the absence of detectable liquid water at 1% RH is in itself ambiguous as to whether these particles have crystallized. However, the extinction spectra for histories 2 and 3 are identical: the full restoration of the condensed-phase water content indicates the absence of crystallization even at 1% RH. (The DRH values of crystalline NH_4HSO_4 and NH_4NO_3 are 40% and 60%, respectively.) The absence of crystallization for aqueous NH_4HSO_4 and NH_4NO_3 particles corroborates literature reports at room temperature.[15,18,25−31]

The spectra collected for the aqueous NH_4HSO_4 and NH_4NO_3 particles reveal changes in the chemical environment of the ions at 1% RH (insets of Figure 3). Aqueous bisulfate peaks occur at 876, 1050, and 1188 cm^{-1}, while a sulfate peak, which arises

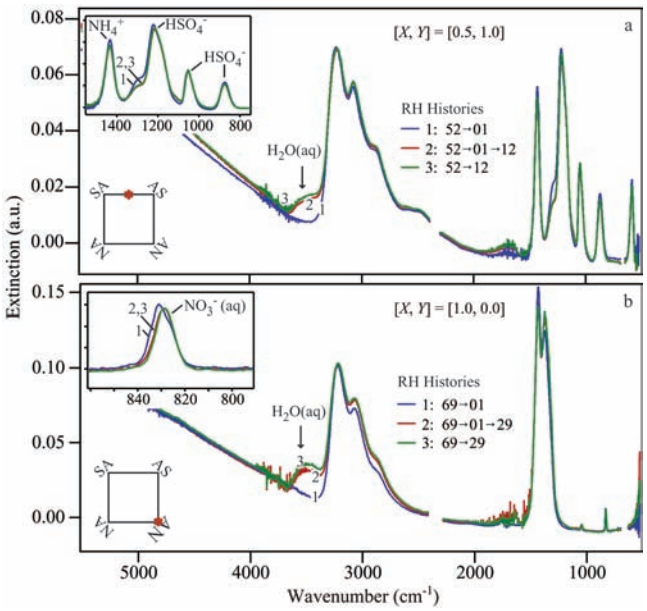

Figure 3. Infrared spectra of aerosol particles exposed to three different RH histories. (a) NH_4HSO_4 (i.e., [0.5, 1.0] composition). (b) NH_4NO_3 (i.e., [1, 0] composition). The uptake of condensed-phase water in both spectra a-2 and b-2 shows that neither aqueous NH_4HSO_4 nor aqueous NH_4NO_3 crystallizes at 293 K, even at 1% RH. (DRH(0.5, 1) = 40%, DRH(1, 0) = 60%.)

from the partial dissociation of HSO_4^-, occurs at 1107 cm^{-1} (Figure 3a, inset). There is an additional peak at 1300 cm^{-1} that does not arise from NH_4^+, HSO_4^-, or SO_4^{2-}, and the intensity of this peak grows at 1% RH compared to 12% RH. We hypothesize that the peak arises from an NH_4^+:::HSO_4^- contact ion pair.[32−34] To our knowledge, although this peak is observable in IR spectra collected previously,[29,35] the present report is the first to indicate that it does not arise from known chemical species and to suggest a contact ion pair.

The infrared spectra of the aqueous NH_4NO_3 aerosol particles show that the degenerate singlet at 830 cm^{-1} of the aqueous $\nu_2(NO_3^-)$ band[36] evolves into an unresolved doublet at 1% RH (Figure 3b, inset). This loss of ion symmetry indicates a change in the solvation environment of NO_3^-, which could arise because of the loss of coordinating H_2O, the approach of NH_4^+ into the solvation shell (i.e., a contact ion pair), or a combination of both of these factors. In addition to the changes observed in the spectra of NH_4HSO_4 [0.5, 1.0] and NH_4NO_3 [1.0, 0] aqueous particles at 1% RH, we also observe changes in the IR spectra of all other [*X*, *Y*] compositions that remain aqueous to 1% RH (Table 1), which we interpret as indicative of changes in the coordination environments of the ions when few H_2O molecules are available.

Whereas some [*X*, *Y*] compositions do not crystallize even at 1% RH, the CRH values of other [*X*, *Y*] compositions can be determined by employing a combination of the extinction spectra and the programming of the aerosol RH history. An example for aerosol particles having a composition [*X*, *Y*] = [1.0, 0.82] is shown in Figure 4. Six $RH_{high} \rightarrow RH_{low} \rightarrow RH_{medium}$ experiments are shown for fixed RH_{high}, variable RH_{low}, and fixed RH_{medium}. For $RH_{low} \leq 31\%$, the IR spectra show that there is no condensed-phase water. Water is apparent, however, for $RH_{low} \geq 34\%$, and the amount of water equals that obtained by a $RH_{high} \rightarrow RH_{medium}$ profile, which rules out any possible suggestion of partial crystallization at 34%. We therefore conclude that 31% < CRH < 34% for [*X*, *Y*] = [1.0, 0.82].

An auxiliary analysis for a CRH determination is by the detection of solid formation via observations of peak splitting

TABLE 1: Initial and Final CRH Values Measured for the [*X*, *Y*] Compositions Studied[a]

	composition [*X*, *Y*]	$DRH_{initial}$	DRH_{final}	$CRH_{initial}$	CRH_{final}
AS pole	[1.0, 1.0]		80		35
	[1.0, 0.82]	66	78		31−34
	[1.0, 0.60]	66	76		26−32
	[1.0, 0.5]	67	75		27−30
3AN·AS pole	[1.0, 0.25]	64	69	1−5	
AN pole	[1.0, 0.00]	62	62		
	[0.85, 1.00]	68	76	26−29	16−24
	[0.85, 0.75]	56	73	27−30	18−23
	[0.85, 0.50]	43	67	13−18	1−13
	[0.70, 1.00]	37	68		19−27
	[0.70, 0.75]	30	63		15−20
	[0.70, 0.50]	36	52	16−18	1−5
	[0.70, 0.25]	29	40		1−4
	[0.70, 0.00]	*b*	48		
AHS pole	[0.50, 1.00]	36	45		
	[0.50, 0.50]	18	20		
	[0.35, 1.00]	*b*	32		
	[0.35, 0.50]	*c*	*c*		
	[0.35, 0.00]	*c*	*c*		

[a] Table entries show upper and lower limit values of the range (e.g., 31% < CRH < 34% for the [1.0, 0.82] composition). Also given are the DRH values of initial water uptake ($DRH_{initial}$) (i.e., eutonic or peritonic composition) and complete solid dissolution (DRH_{final}). The DRH values are based on the AIM thermodynamic model.[12] [b] A solid is in equilibrium with an aqueous acidic solution even at low RH. [c] A solid is not thermodynamically favored even at low RH; an acidic liquid phase is favored.

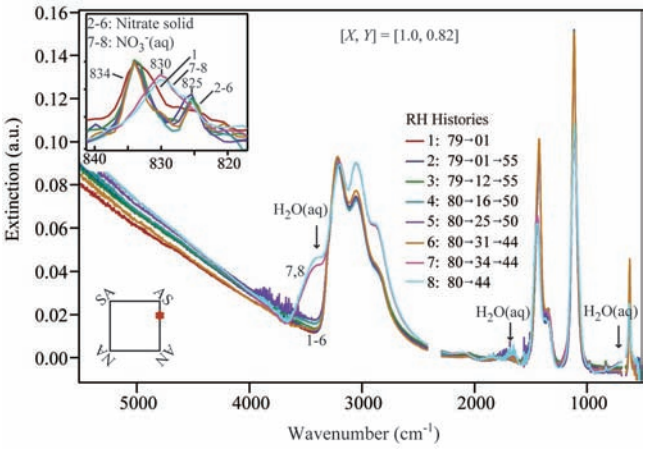

Figure 4. Determination of CRH value at 293 K for aerosol particles having composition [1.0, 0.82]. Spectra for particles exposed to eight different RH histories are shown. Condensed-phase water is present in spectrum 7 (80 → 34 → 44) but is absent in spectrum 6 (80 → 31 → 44). We therefore conclude that 31% < CRH < 34%. The inset shows that the peak for NO_3^-(aq) splits into a doublet of 825 and 834 cm^{-1}, which is diagnostic for the formation of 2AN·AS. ($DRH_{initial}$(1, 0.82) = 66% and DRH_{final}(1, 0.82) = 78% for the equilibrium path predicted by the AIM model.[12])

characteristic of particular crystals. The inset in Figure 4 shows an example. The aqueous nitrate peak at 830 cm^{-1} is present in the spectra of particles that do not crystallize ($RH_{low} \geq 34\%$). When crystallization occurs, peaks appear at 825 and 834 cm^{-1} and disappear at 830 cm^{-1}. The new peaks are characteristic of crystalline 2AN·AS (cf. section 3.2).

The approach outlined in Figure 4 is applied to determine the CRH values at 293 K of 19 different [*X*, *Y*] compositions to provide a representative mapping of the crystallization behavior of the $SO_4^{2-}-NO_3^--NH_4^+-H^+$ system. The results are summarized in Table 1. Fitting functions for the CRH(*X*,*Y*) results

TABLE 2: Spectral Assignments for Crystals Formed[a]

peak position	species	AS	LET	AHS	2AN·AS	3AN·AS	AN	AN·AHS	aqueous	quality[b]
590	HSO_4^-			M[c]				M	M	ambiguous
596	HSO_4^-		M					M		unique
619	SO_4^{2-}	M		M	M	M			M	ambiguous
715	NO_3^-							W		
725	NO_3^-							W		
821	NO_3^-					W		W		unique
825	NO_3^-				W					unique
830	NO_3^-					W	W		W	ambiguous
834	NO_3^-				W					unique
855	HSO_4^-							M		
864	HSO_4^-		M	M						ambiguous
876	HSO_4^-								M	ambiguous
883	HSO_4^-		M	M						ambiguous
975	SO_4^{2-}	W								unique
1020	HSO_4^-		M	M						ambiguous
1050	HSO_4^-			M				M	M	ambiguous
1050	NO_3^-						W		W	ambiguous
1060	HSO_4^-							M		
1084	SO_4^{2-}				S	S		M		ambiguous
1095	HSO_4^{2-}		S	S						ambiguous
1115	SO_4^{2-}	S							S	ambiguous
1134	SO_4^{2-}		S	S						ambiguous
1188	HSO_4^-		S	S					S	ambiguous
1208	HSO_4^-		S	S				M		ambiguous
1242	HSO_4^-							M		
1333	NO_3^-				S	S	S	M	S	ambiguous
1365	NO_3^-				S	S	S	S	S	ambiguous
1426	NH_4^+	S	S	S	S	S	S	S	S	ambiguous
1451	NH_4^+	S	S	S	S	S	S	M	S	ambiguous
confidence		very high[24,52]	high[53,54]	high[29,55]	this study	this study	very high[55−57]	this study	very high[58−61]	

[a] Peak positions are approximate (± 3 cm^{-1} in most cases and ± 6 cm^{-1} for AN·AHS measured by DRIFTS), and there are slight shifts of a given peak (e.g., 619 and 830 cm^{-1}) among the different crystals. To our knowledge, our reported IR spectra of 2AN·AS (aerosol), 3AN·AS (aerosol), and AN·AHS (DRIFTS) are new. [b] Our designation "ambiguous" indicates the peak is shared by two or more crystals or with the aqueous phase; the designation "unique" indicates the peak is diagnostic of a particular crystal. (We omit AN·AHS from the comparison set for "unique" because this crystal is not observed in any of our aerosol experiments.) [c] Peak intensities are classified as weak (W), medium (M), and strong (S).

and graphical depictions of the CRH(X,Y) surface were previously reported.[15] The solid line in the upper-left panel of Figure 9a shows the dividing line between [X, Y] compositions that do and do not crystallize, even at 1% RH. Particles having compositions close to that of ammonium sulfate have the highest CRH values; increasing either nitrate content or acidity decreases the CRH value. Seven of the studied compositions do not crystallize even at 1% RH. When crystallization does occur, $40\% < \Delta\mathrm{RH}(X,Y) < 55\%$ for most cases, where $\Delta\mathrm{RH}(X,Y) \equiv (\mathrm{DRH}(X,Y) - \mathrm{CRH}(X,Y))$.

For several compositions away from crystal poles (e.g., [1, 1] for AS or [0.75, 1] for LET), we observe an initial crystallization at an elevated $\mathrm{RH_{low}}$, which is then followed by a complete crystallization at a lower $\mathrm{RH_{low}}$. Table 1 summarizes these results as $\mathrm{CRH_{initial}}$ and $\mathrm{CRH_{final}}$. For $\mathrm{RH_{low}} < \mathrm{CRH_{final}}$, the condensed-phase water content is below detection for $\mathrm{RH_{high}} \rightarrow \mathrm{RH_{low}} \rightarrow \mathrm{RH_{medium}}$ (cf. Figures 2 and 4), which we interpret as the complete crystallization of all aerosol particles. In contrast, for $\mathrm{CRH_{final}} < \mathrm{RH_{low}} < \mathrm{CRH_{initial}}$, there is a decrease in the condensed-phase water for a program of $\mathrm{RH_{high}} \rightarrow \mathrm{RH_{low}} \rightarrow \mathrm{RH_{medium}}$ compared to one of $\mathrm{RH_{high}} \rightarrow \mathrm{RH_{medium}}$. It may be that the aerosol at $\mathrm{CRH_{initial}}$ consists of an external mixture of completely crystalline versus aqueous particles. If so, the implication is that the slope $\mathrm{d}J/\mathrm{d}(a_{\mathrm{H_2O}})$ is shallower than normal and that an increased residence time would lead to a greater extent of crystallization, where J is the homogeneous nucleation rate and $a_{\mathrm{H_2O}}$ is the aqueous water activity.[13] Alternatively, the aerosol at $\mathrm{CRH_{initial}}$ may contain internally mixed particles, in which each individual particle has crystalline and aqueous components.[37−39]

3.2. Crystals Formed. The solids formed upon crystallization of aerosol particles can be identified from their spectroscopic signatures in the range 580−1550 cm^{-1} (Table 2). In the case of AS, the aerosol spectroscopic signature is well-known, including peak positions, widths, and intensities. In other cases, including AHS, LET, and AN, the spectroscopic signatures are available only as transmission measurements, and there are some differences between aerosol extinction and transmission measurements of the same material, such as peak shifts due to differing contributions of the real and imaginary components of the refractive index to the observation. In other cases, including 2AN·AS and 3AN·AS, the spectroscopic signatures have not been previously recorded, and we must infer these signatures from our collected data. To do so, we analyze the subset of recorded spectra corresponding to complete crystallization at 1% RH, and we employ *Mathematica* to fit the spectra with Lorentzian curves, including global constraints on peak positions, widths, and intensities. The results of our analysis are summarized in Table 2.

An example of the crystallization of AS and LET from aqueous aerosol particles having a composition of [0.85, 1.0] is shown in Figure 5. Significant spectral differences are apparent between the upper ($\mathrm{RH_{high}} \rightarrow \mathrm{RH_{medium}}$; Figure 5a) and lower ($\mathrm{RH_{high}} \rightarrow \mathrm{RH_{low}} \rightarrow \mathrm{RH_{medium}}$; Figure 5b) sides of the hysteresis loop. As shown in Table 2 and Figure 5b, several of the peaks on the lower side of the hysteresis loop are uniquely assignable to AS or LET, while other peaks such as the ammonium vibrations are common to both crystals. Moreover, the absence of a sharp peak at 1050 cm^{-1} is evidence that no detectable AHS forms.

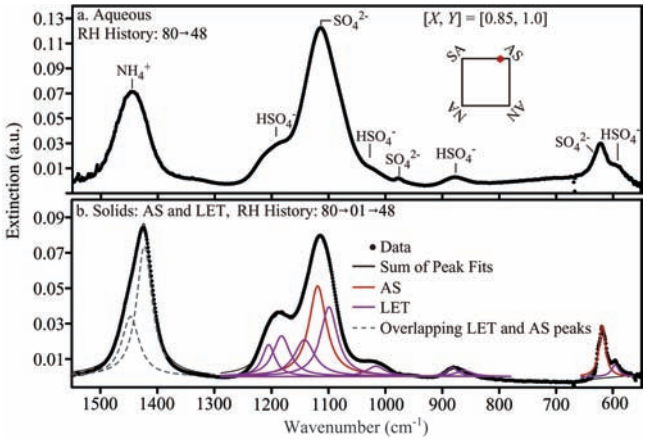

Figure 5. Infrared spectra of (a) aqueous and (b) solid aerosol particles of composition $[X, Y] = [0.85, 1.0]$. Peak fits are shown in part b.

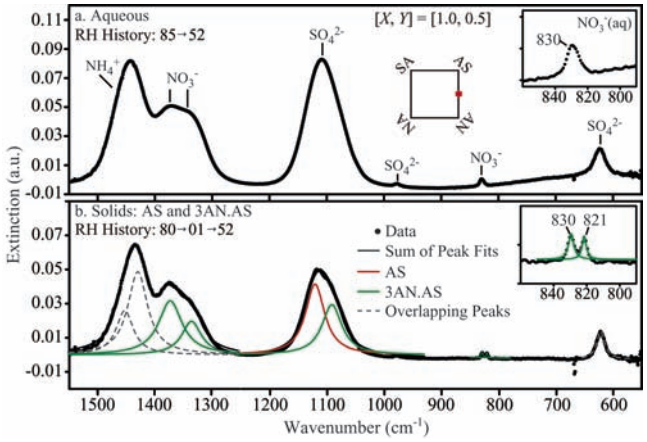

Figure 6. Infrared spectra of (a) aqueous and (b) solid aerosol particles of composition $[X, Y] = [1.0, 0.5]$. Peak fits are shown in part b.

An example similar to Figure 5, but now for the crystallization of AS and 3AN·AS from aqueous aerosol particles having a composition of [1.0, 0.5], is shown in Figure 6. Significant spectral differences are apparent between the upper and the lower sides of the hysteresis loop (Figure 6a versus 6b). Strikingly, the 830 cm^{-1} nitrate peak splits into two sharp peaks: the 821 and 830 cm^{-1} peaks are signatures of 3AN·AS. We believe our reports of the spectral characteristics of this crystal and of the formation of this crystal in aerosol particles are the first of their kind.

Whereas the two previous examples (Figures 5 and 6) are constrained to the $[X, 1]$ and $[1, Y]$ axes, an off-axis example showing the crystallization of LET, AHS, AS, and AN from aqueous aerosol particles having a composition of [0.7, 0.75] is shown in Figure 7. Particles of this composition are composed of sulfate, nitrate, ammonium, and proton, so both sulfate and nitrate crystals are possible. LET, AHS, AS, and AN precipitate. The sharp 830 cm^{-1} peak is characteristic of AN: crystalline ammonium nitrate forms in an initially homogeneous aerosol particle. Because aerosol particles of pure aqueous NH_4NO_3 do not crystallize, we infer that one of AS or LET is a good heterogeneous nucleus for AN. Previously, mineral dust[31] and crystalline succinic acid[30] inclusions inside aerosol particles have also been shown to induce AN crystallization. Similarly, pure aqueous NH_4HSO_4 aerosol particles do not crystallize. We therefore conclude that one of LET or AS precipitates first, followed by the heterogeneous nucleation of AHS and AN.

The Gibbs phase rule allows a maximum of three solids to form for off-axis $[X, Y]$ compositions, yet we report four solids

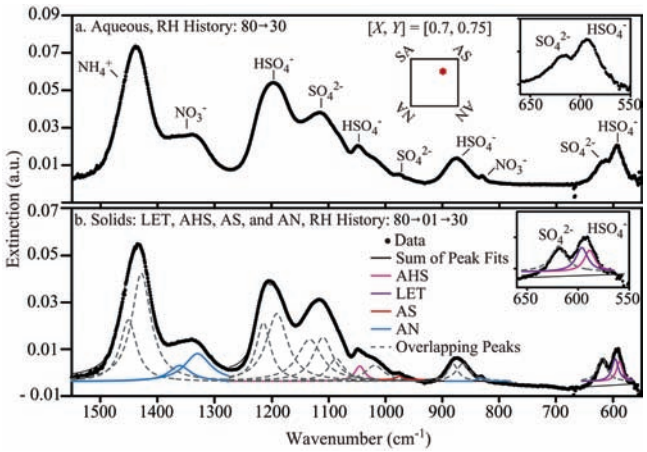

Figure 7. Infrared spectra of (a) aqueous and (b) solid aerosol particles of composition $[X, Y] = [0.7, 0.75]$. Peak fits are shown in part b.

for the composition of [0.7, 0.75]. The implication is that an externally mixed aerosol forms. The combination of the requirements of LET or AS in particles (to serve as heterogeneous nuclei), of an average composition of [0.7, 0.75] in each particle, and of the Gibbs phase rule leads to the conclusion that individual particles are of type 1 (15% AS, 60% AHS, 25% AN) or type 2 (35% LET, 45% AHS, 25% AN). The requirements do not constrain the ratio of type 1 to type 2 particles. Other $[X, Y]$ compositions having externally mixed populations are noted in Table 3.

The crystallization mechanisms of aqueous particles having chemical compositions different from the crystals formed can be complex. Namely, histories of $RH_{high} \rightarrow RH_{low}$ compared to those of $RH_{high} \rightarrow RH_{low} \rightarrow RH_{medium}$ for $RH_{low} = 1\%$ yield different crystals for some $[X, Y]$ compositions. An example for aerosol particles having a composition of [1.0, 0.60] is shown in Figure 8. Although the aerosol particles are crystalline for both 80 → 1% RH and 80 → 1 → 40% RH (Figure 8a), the crystals present are different. At 1% RH, the particles are composed of AS and 3AN·AS (Figure 8b). In comparison, AS and 2AN·AS are predicted thermodynamically. Increasing RH to 40% changes the mix of crystals to 3AN·AS, 2AN·AS, and AS (Figure 8c). Because the Gibbs phase rule allows only two solids for [1.0, 0.6], the implication is that a uniform aerosol population of {47% AS, 53% 3AN·AS} metastable particles at 1% RH changes at 40% RH to a mixed population of {47% AS, 53% 3AN·AS} metastable particles and {40% AS, 60% 2AN·AS} stable particles.

To explain the complex effect of RH history on the crystals formed, we hypothesize that metastable crystals nucleate first at $a_{H_2O} = 0.01$, as predicted by Ostwald's rule of stages.[40] We hypothesize that enough water is surface-adsorbed at RH_{medium} that ions have sufficient mobility[41] so the metastable crystals can transform into the thermodynamically stable forms. Analogies can be made between this explanation of the effects of RH history and theories of the effects of temperature programming (i.e., quenching and annealing) in materials processing. In support of our explanation, Table 3 summarizes the thermodynamic predictions of crystals formed to those actually observed at 1% RH and at RH_{medium}. For compositions such as [0.70, 0.75] or [0.70, 0.50], a uniform aerosol population (i.e., internally mixed) composed of metastable phases forms at 1% RH but transforms into a mixed aerosol population (i.e., externally mixed) at higher RH. This explanation implies that only a fraction of the aerosol particles transforms at RH_{medium}. We speculate, without ruling out other possibilities, that critical

TABLE 3: Comparison of Crystals Predicted by AIM Thermodynamic Model[12] to Those Observed in Our Measurements for RH Histories of $RH_{high} \rightarrow 1$ and $RH_{high} \rightarrow 1 \rightarrow RH_{medium}$[a]

composition [*X*, *Y*]	AIM prediction	our results $RH_{high} \rightarrow 1\%$	our results (RH_{medium}) $RH_{high} \rightarrow 1\% \rightarrow RH_{medium}$
[1.0, 1.0]	AS	AS	AS ($RH_{medium} = 70$)
[1.0, 0.82]	AS, 2AN·AS	AS, 2AN·AS	AS, 2AN·AS (55)
[1.0, 0.60]	AS, 2AN·AS	AS, *3AN·AS*	AS, 2AN·AS, *3AN·AS*[b] (41)
[1.0, 0.50]	AS, 2AN·AS	AS, *3AN·AS*	AS, *3AN·AS* (52)
[1.0, 0.25]	3AN·AS	2AN.AS, 3AN·AS[b]	2AN·AS, 3AN·AS[b] (40)
[1.0, 0.0]	AN	no crystal	no crystal
[0.85, 1.00]	AS, LET	AS, LET	AS, LET (48)
[0.85, 0.75]	AS, LET, 2AN·AS	AS, LET[c]	AS, LET, 2AN·AS (30)
[0.85, 0.50]	LET, AN, 3AN·AS	*AS*, LET, AN	*AS*, LET, *2AN·AS* (12)
[0.70, 1.00]	LET, AHS	LET, AHS, *AS*[b]	LET, AHS, *AS*[b] (30)
[0.70, 0.75]	LET, AHS, AN·AHS	LET, AHS, *AN*	LET, *AS*, AHS, *AN*[b] (30)
[0.70, 0.50]	LET, AN, AN·AHS	LET, *AHS*, AN	LET, *AS*, *AHS*, AN[b] (30)
[0.70, 0.25]	AN, AN·AHS	AN[c]	*2AN·AS*[c] (24)
[0.70, 0.00]	AN, aqueous	no crystal	no crystal
[0.50, 1.00]	AHS	no crystal	no crystal
[0.50, 0.50]	AHS, AN·AHS, aqueous	no crystal	no crystal
[0.35, 1.00]	no crystal	no crystal	no crystal
[0.35, 0.50]	no crystal	no crystal	no crystal
[0.35, 0.00]	no crystal	no crystal	no crystal

[a] The differences between the predictions and the observations are in italics. Unresolved crystals (q.v. Figure 9) are not included in the comparison. Although AN·AHS is predicted in many cases, we never find spectral evidence for its occurrence in the aerosol spectra. [b] The Gibbs phase rule requires an aerosol having two separate particle populations (i.e., externally mixed). [c] There are additional solids present (q.v. Figure 9), but they cannot be unambiguously identified by the collected infrared spectra. These additional solids allow the Gibbs phase rule to be satisfied for a homogeneous aerosol population (i.e., internally mixed).

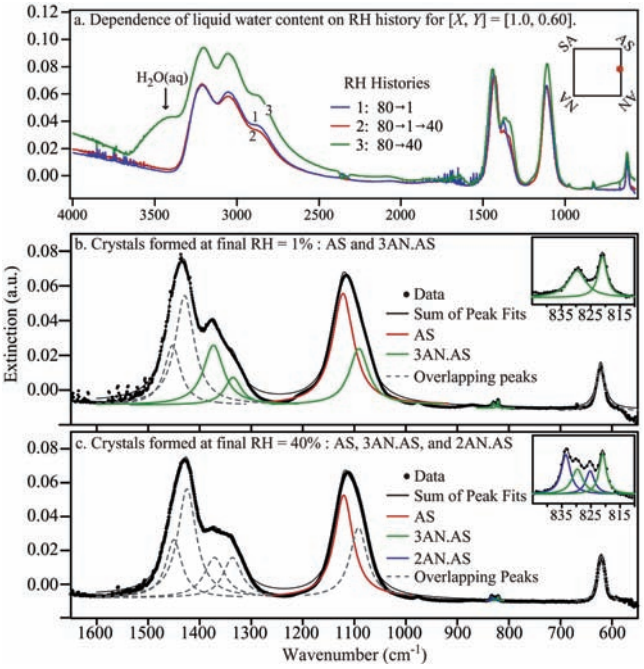

Figure 8. For [*X*, *Y*] = [1.0, 0.6], the crystals formed at 1% RH are different from those at 40% RH. (a) Spectral evidence that aerosol particles are crystalline both at 1% and 40% RH. There is an absence of condensed-phase water for RH histories of 80 → 1 and 80 → 1 → 40. (b, c) Crystals formed at 1% versus 40% RH.

germs (having mass too small for detection in our infrared extinction measurements) stochastically form at 1% RH in a fraction of the particles and that these particles then recrystallize at higher RH when adsorbed water facilitates ion movement.

The crystals formed at the studied [*X*, *Y*] compositions are summarized in Figure 9 for histories of (a) $RH_{high} \rightarrow 1\%$ and (b) $RH_{high} \rightarrow 1\% \rightarrow RH_{medium}$. In some of the infrared spectra, the presence or absence of specific solids could not be unambiguously determined; these cases are shown as solid gray squares in Figure 9. The most prevalent example of this ambiguity is AS, which has few IR absorptions because of the high symmetry of NH_4^+ and SO_4^{2-} (i.e., tetrahedral) and those few IR absorptions overlap with peaks of 2AN·AS, 3AN·AS, and LET. Ambiguities also occur for the nitrate-bearing crystals for several of the off-axis [*X*, *Y*] compositions because discrimination among the unique but weak nitrate peaks over the range 821−835 cm^{-1} is made difficult by the tail of the 864 cm^{-1} HSO_4^- peak. Figure 9 also shows that AHS occurs only when LET is also present; we infer that LET is a good heterogeneous nucleus for AHS.

3.3. Atmospheric Implications. Our new laboratory results show that AN and AHS crystals form more readily in SNA particles than previously believed[15,18,25−31] and, therefore, could be more widespread in SNA-dominant aerosol particles in the troposphere than previously anticipated. Our results show that compositions enriched in NO_3^- or H^+ crystallize via heterogeneous pathways at conditions of sufficiently low RH. For example, LET and AS can serve as heterogeneous nuclei for both AN and AHS, crystals which do not crystallize homogeneously at 293 K. Therefore, the rule that has emerged from laboratory studies that AN and AHS do not crystallize in inclusion-free aerosol particles above 273 K[13,15,18,25−31] must now be relaxed: an initially aqueous particle can form AN or AHS if AS or LET crystallizes first, assuming the remaining liquid phase is saturated with respect to AN or AHS.

Crystals of 2AN·AS and 3AN·AS, which are given scant attention in the literature of atmospheric aerosols,[42] could also be much more widespread in the troposphere than currently considered. Our laboratory results show that aqueous NO_3^- can crystallize as 2AN·AS or 3AN·AS, provided sufficient aqueous sulfate is present. Tani et al. report that 2AN·AS and 3AN·AS are common crystals in atmospheric particles, at least those collected at a roadside station at Argonne National Laboratory in the winter.[43]

Much more future work is needed on the temperature dependence of our results (limited to 293 K) and their implications so that predictions relevant to the full range of tropospheric temperatures will be possible. Literature reports concerning the

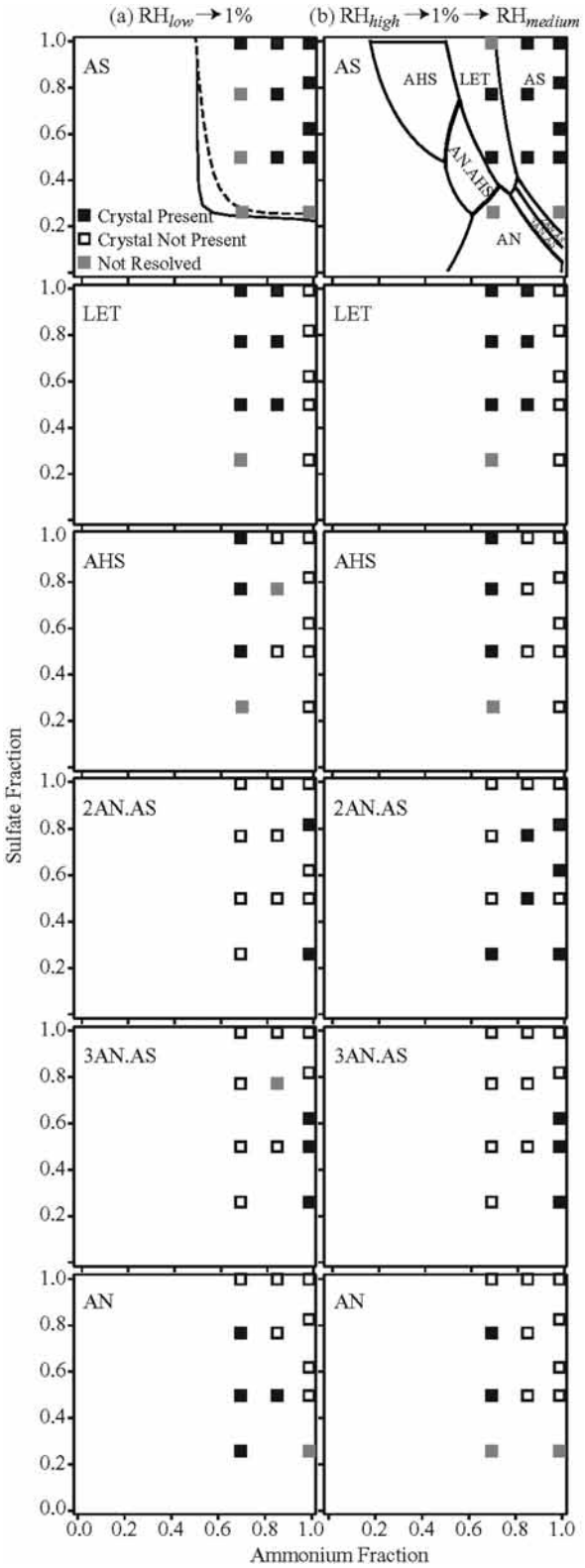

Figure 9. Summary of crystals formed at the studied [*X*, *Y*] compositions for histories of (a) $RH_{high} \rightarrow 1\%$ and (b) $RH_{high} \rightarrow 1\% \rightarrow RH_{medium}$. Black squares indicate that a particular crystal is present, open squares indicate that the crystal is not present, and gray squares indicate that the presence or absence of the crystal cannot be resolved using the spectroscopic data. Also shown in the top row are (left) a line separating those compositions that do and do not crystallize[15] even at 1% RH and (right) the thermodynamic phase diagram[6] for the crystals of the $SO_4^{2-}-NO_3^{-}-NH_4^{+}-H^{+}$ system at 293 K.

temperature dependence of crystallization can, however, begin to provide some guidance. Crystallization of aqueous ammonium sulfate particles (i.e., [1,1]) depends slightly, if at all, on temperature from 234 to 298 K.[19,44] Furthermore, Czizco and Abbatt[29] report that aqueous ammonium bisulfate and aqueous ammonium nitrate particles do not crystallize from 238 to 298 K. There are no other systematic studies of the temperature dependence of the crystallization of other [*X*, *Y*] compositions. Some insight can be gained along the [*X*, 1] axis, however, by comparison of our results for crystals formed at 293 K with those of Colberg et al. at 264 K.[39] We both report the formation of LET near [0.75, 1] and at similar CRH values, thus indicating an absence of temperature dependence for that composition. In contrast, whereas we observe no crystallization at room temperature for particles of composition [0.5, 1], Colberg et al. report that LET forms at 16% RH at 264 K. The report by Colberg et al. could suggest that the $X-Y$ region having CRH $> 1\%$ for LET is larger at 264 K than at 293 K. The differences in the temperature dependence of the CRH values of AS versus LET (i.e., no dependence for AS at [1, 1] versus a strong dependence for LET at [0.5, 1]) are also reflected in the weak and strong temperature dependencies, respectively, of the liquidus curves (i.e., the DRH_{final} values) of these solids.[13] The surety of the conclusion that the CRH value of particles of [0.5, 1] composition is temperature dependent must, however, be tempered by an apparent outstanding contradiction between the report by Colberg et al. of the formation of LET from aqueous [0.5, 1] particles and the report by Czizco and Abbatt of an absence of crystal formation, even to 238 K. Particle diameter is one readily identifiable difference between the two studies, namely 2−20 μm for Colberg et al. and 0.36 μm for Czizco and Abbatt. Particle size could thus play an important role in crystallization behavior. Further work is necessary to understand the effect of size and temperature on crystallization behavior.

An additional uncertainty arises in the extrapolation of our laboratory results obtained for the crystallization of SNA aerosol particles to implications for the crystallization behavior of SNA-dominant aerosol particles. There are several recent publications concerning the effects of organic molecules on the crystallization of inorganic aerosol particles. Choi and Chan showed that for mixtures of $(NH_4)_2SO_4$ and organic molecules in a 1:1 mole ratio, succinic, malonic, and glutaric acids increased the CRH of AS, while glycerol caused the CRH to decrease.[45] In contrast, Pant et al. found that the CRH of mixed $(NH_4)_2SO_4$−glutaric acid particles was slightly lower than that of pure AS up to a glutaric acid mole fraction of 0.4 before significantly decreasing at higher mole fractions,[11] in agreement with the discussion offered in Martin et al.[15] In contrast to Choi and Chan, Braban and Abbatt reported that malonic acid decreases the CRH of AS.[46] In short, depending upon their specific chemical nature, organic molecules can increase, leave unchanged, or decrease the CRH of SNA-dominant particles.[6] There are also several studies on the effects of organic molecules on the deliquescence of SNA-dominant particles.[47−49,50] Further work on the effects of organic molecules is warranted. The effects of insoluble cores such as mineral dust particles, which are coated by SNA layers, have established that heterogeneous nucleation can significantly increase the CRH of aqueous SNA layers.[20,31,51]

4. Conclusions

The crystals formed at 293 K by aqueous sulfate−nitrate−ammonium−proton aerosol particles have been identified. The six crystals include AS, 2AN·AS, 3AN·AS, AN, LET, and AHS. The infrared aerosol spectroscopic signatures of these crystals are delineated. Our reports both of the infrared spectroscopic

signatures of 2AN·AS and 3AN·AS and of their formation in aerosol particles are the first we know of. Our report of the formation of AHS and AN in aerosol particles from initially aqueous particles is also the first we know of: the crystallization occurs via heterogeneous nucleation on AS or LET for aqueous particles having compositions different from the pure species (i.e., more neutralized than NH_4HSO_4(aq) or more sulfate-containing than NH_4NO_3(aq)). The implication of these results is that these solid phases may be more widespread in the troposphere than currently considered in the literature, although further studies on the effects of temperature, particle size, and other chemical constituents of ambient aerosol are needed for more accurate predictions.

The crystallization pathways of aqueous sulfate−nitrate−ammonium−proton aerosol particles are complex. As an example, the formation of one crystal such as LET inside an aerosol particle can lead to the heterogeneous nucleation of another such as AHS. As a second example, whereas a uniform population of metastable aerosol particles forms at 1% RH, this population can transform into a mix of metastable and stable particles at higher relative humidity (i.e., an externally mixed aerosol).

Knowledge of the crystals formed by aqueous sulfate−nitrate−ammonium−proton aerosol particles can be incorporated into atmospheric chemical transport models to improve the accuracy of particle phase prediction and the understanding of the effect of aerosol particle phase on radiative forcing and atmospheric chemical reactions. Uncertainties of the effects of aerosol particles on climate can thereby be reduced.

Acknowledgment. We are grateful for support received from the NSF Atmospheric Chemistry Program (ATM-0317583).

References and Notes

(1) Penner, J. E.; Andreae, M.; Annegarn, H.; Barrie, L.; Feichter, J.; Hegg, D.; Jayaraman, A.; Leaitch, R.; Murphy, D.; Nganga, J.; Pitari, G. Aerosols, their Direct and Indirect Effects. In *In Climate Change 2001: The Scientific Basis. Contribution of Working Group I to the Third Assessment Report of the Intergovernmental Panel on Climate Change*; Houghton, J. T., Ding, Y., Griggs, D. J., Noguer, M., Linden, P. J., Dai, X., Maskell, K., Johnson, C. A., Eds.; Cambridge University Press: New York, 2001; p 289.

(2) Hegg, D.; Larson, T.; Yuen, P. F. *J. Geophys. Res.* **1993**, *98*, 18435.

(3) Dentener, F. J.; Crutzen, P. J. *J. Geophys. Res.* **1993**, *98*, 7149.

(4) Tie, X. X.; Emmons, L.; Horowitz, L.; Brasseur, G.; Ridley, B.; Atlas, E.; Stround, C.; Hess, P.; Klonecki, A.; Madronich, S.; Talbot, R.; Dibb, J. *J. Geophys. Res.* **2003**, *108*, 8364.

(5) Colberg, C. A.; Luo, B. P.; Wernli, H.; Koop, T.; Peter, T. *Atmos. Chem. Phys.* **2003**, *3*, 909.

(6) Martin, S. T.; Hung, H. M.; Park, R. J.; Jacob, D. J.; Spurr, R. J. D.; Chance, K. V.; Chin, M. *Atmos. Chem. Phys.* **2004**, *4*, 183.

(7) Seinfeld, J. H.; Pandis, S. N. *Atmospheric Chemistry and Physics: From Air Pollution to Climate Change*; Wiley: New York, 1998.

(8) Thornton, J. A.; Braban, C. F.; Abbatt, J. P. D. *Phys. Chem. Chem. Phys* **2003**, *5*, 4593.

(9) Hallquist, M.; Stewart, D. J.; Stephenson, S. K.; Cox, R. A. *Phys. Chem. Chem. Phys* **2003**, *5*, 3453.

(10) Schwartz, S.; Freiberg, J. *Atmos. Environ.* **1981**, *15*, 1129.

(11) Pant, A.; Fok, A.; Parsons, M. T.; Mak, J.; Bertram, A. K. *Geophys. Res. Lett.* **2004**, *31*, L12111.

(12) Clegg, S. L.; Brimblecombe, P.; Wexler, A. S. *J. Phys. Chem. A* **1998**, *102*, 2137.

(13) Martin, S. T. *Chem. Rev.* **2000**, *100*, 3403.

(14) Nenes, A.; Pandis, S. N.; Pilinis, C. *Aquat. Geochem.* **1998**, *4*, 123.

(15) Martin, S. T.; Schlenker, J. C.; Malinowski, A.; Hung, H. M.; Rudich, Y. *Geophys. Res. Lett.* **2003**, *30*, 2102.

(16) Rood, M. J.; Larson, T. V.; Covert, D. S.; Ahlquist, N. C. *Atmos. Environ.* **1985**, *19*, 1181.

(17) Tang, I. N. Deliquescence properties and particle size change of hygroscopic aerosols. In *Generation of Aerosols and Facilities for Exposure Experiments*; Willeke, K., Ed.; Ann Arbor Science Publishers: Ann Arbor, 1980.

(18) Cziczo, D. J.; Nowak, J. B.; Hu, J. H.; Abbatt, J. P. D. *J. Geophys. Res.* **1997**, *102*, 18843.

(19) Onasch, T. B.; Siefert, R. L.; Brooks, S. D.; Prenni, A. J.; Murray, B.; Wilson, M. A.; Tolbert, M. A. *J. Geophys. Res.* **1999**, *104*, 21317.

(20) Han, J. H.; Martin, S. T. *J. Geophys. Res.* **1999**, *104*, 3543.

(21) Hung, H. M.; Malinowski, A.; Martin, S. T. *J. Phys. Chem. A* **2002**, *106*, 293.

(22) Chelf, J. H.; Martin, S. T. *J. Geophys. Res.* **2001**, *106*, 1215.

(23) Hung, H. M.; Malinowski, A.; Martin, S. T. *J. Phys. Chem. A* **2003**, *107*, 1296.

(24) Weis, D. D.; Ewing, G. E. *J. Geophys. Res.* **1996**, *101*, 18709.

(25) Tang, I. N.; Munkelwitz, H. R. *J. Aerosol Sci.* **1977**, *8*, 321.

(26) Richardson, C. B.; Hightower, R. L. *Atmos. Environ.* **1987**, *21*, 971.

(27) Tang, I. N.; Munkelwitz, H. R. *J. Geophys. Res.* **1994**, *99*, 18801.

(28) Dougle, P. G.; Veefkind, J. P.; ten Brink, H. M. *J. Aerosol. Sci.* **1998**, *29*, 375.

(29) Cziczo, D. J.; Abbatt, J. P. D. *J. Phys. Chem. A* **2000**, *104*, 2038.

(30) Lightstone, J. M.; Onasch, T. B.; Imre, D.; Oatis, S. *J. Phys. Chem. A* **2000**, *104*, 9337.

(31) Han, J. H.; Hung, H. M.; Martin, S. T. *J. Geophys. Res.* **2002**, *107*, 4086.

(32) Zhang, Y. H.; Chan, C. K. *J. Phys. Chem. A* **2002**, *106*, 285.

(33) Zhang, Y. H.; Chan, C. K. *J. Phys. Chem. A* **2000**, *104*, 9191.

(34) Zhang, Y. H.; Choi, M. Y.; Chan, C. K. *J. Phys. Chem. A* **2004**, *108*, 1712.

(35) Han, J. H.; Martin, S. T. *Aerosol Sci. Technol.* **2001**, *34*, 363.

(36) Nakamoto, K. *Infrared and Raman Spectra of Inorganic and Coordination Compounds*, 4th ed.; Wiley: New York, 1986.

(37) Weis, D. D.; Ewing, G. E. *J. Geophys. Res.* **1999**, *104*, 21275.

(38) Braun, C.; Krieger, U. K. *Opt. Express.* **2001**, *8*, 314.

(39) Colberg, C. A.; Krieger, U. K.; Peter, T. *J. Phys. Chem. A* **2004**, *108*, 2700.

(40) Markov, I. V. *Crystal Growth for Beginners*; World Scientific: Singapore, 1995.

(41) Finlayson-Pitts, B. J. *Chem. Rev.* **2003**, *103*, 4801.

(42) Wexler, A. S.; Clegg, S. L. *J. Geophys. Res.* **2002**, *107*, 4207.

(43) Tani, B.; Siegel, S.; Johnson, S. A.; Kumar, R. *Atmos. Environ.* **1983**, *17*, 2277.

(44) Cziczo, D. J.; Abbatt, J. P. D. *J. Geophys. Res.* **1999**, *104*, 13781.

(45) Choi, M. Y.; Chan, C. K. *Environ. Sci. Technol.* **2002**, *36*, 2422.

(46) Braban, C. F.; Abbatt, J. P. D. *Atmos. Chem. Phys.* **2004**, *4*, 1451.

(47) Brooks, S. D.; Wise, M. E.; Cushing, M.; Tolbert, M. A. *Geophys. Res. Lett.* **2002**, *29*, 4487.

(48) Braban, C. F.; Carroll, M. F.; Styler, S. A.; Abbatt, J. P. D. *J. Phys. Chem. A* **2003**, *107*, 6594.

(49) Parsons, M. T.; Mak, J.; Lipetz, S. R.; Bertram, A. K. *J. Geophys. Res.* **2004**, *109*, D06212.

(50) Marcolli, C.; Luo, B.; Peter, T. *J. Phys. Chem. A* **2004**, *108*, 2216.

(51) Martin, S. T.; Han, J. H.; Hung, H. M. *Geophys. Res. Lett.* **2001**, *28*, 2601.

(52) Toon, O. B.; Pollack, J. B.; Khare, B. N. *J. Geophys. Res.* **1976**, *81*, 5733.

(53) Damak, M.; Kamoun, M.; Daoud, A.; Romain, F.; Lautie, A.; Novak, A. *J. Mol. Struct.* **1985**, *130*, 245.

(54) Kamoun, M.; Lautie, A.; Romain, F.; Novak, A. *J. Raman Spectrosc.* **1988**, *19*, 329.

(55) Miller, F. A.; Wilkins, C. H. *Anal. Chem.* **1952**, *24*, 1253.

(56) Kearley, G. J.; Kettle, S. F. A. *J. Chem. Phys.* **1980**, *73*, 2129.

(57) Jarzembski, M. A.; Norman, M. L.; Fuller, K. A.; Srivastava, V.; Cutten, D. R. *Appl. Opt.* **2003**, *42*, 922.

(58) Marcus, R. A.; Fresco, J. M. *J. Chem. Phys.* **1957**, *27*, 564.

(59) Giguere, P. A.; Savoie, R. *J. Am. Chem. Soc.* **1963**, *85*, 287.

(60) Querry, M. R.; Waring, R. C.; Holland, W. E.; Earls, L. M.; Herrman, M. D.; Nijm, W. P.; Hale, G. M. *J. Opt. Soc. Am.* **1974**, *64*, 39.

(61) Martin, S. T.; Salcedo, D.; Molina, L. T.; Molina, M. J. *J. Phys. Chem. B* **1997**, *101*, 5307.